

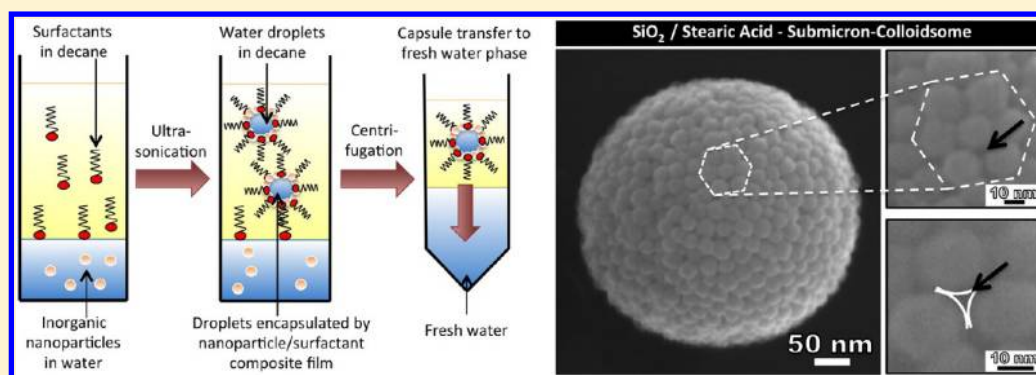
Synthesis Route for the Self-Assembly of Submicrometer-Sized Colloidosomes with Tailorable Nanopores

Tobias Bollhorst,[†] Tim Grieb,[‡] Andreas Rosenauer,[‡] Gerald Fuller,[§] Michael Maas,^{*,†} and Kurosch Rezwan[†]

[†]Advanced Ceramics, University of Bremen, Am Biologischen Garten 2, D-28359 Bremen, Germany

[‡]Institute of Solid State Physics, University of Bremen, Otto-Hahn-Allee 1, D-28359 Bremen, Germany

[§]Department of Chemical Engineering, Stanford University, Stanford, California 94305-5025, United States



ABSTRACT: We present a synthesis route to fabricate submicrometer-sized colloidosomes at ambient conditions and mild pH with tailorable nanopore sizes and porosity. The capsules are formed via self-assembly of metal oxide nanoparticles on emulsion droplets in a water-in-oil emulsion. Through the adsorption of oil-soluble surfactants on emulsion droplets, which carry the same sign of charge as the colloidosome-forming particles in aqueous media, colloidosomes with positive and negative zeta potentials were synthesized. The hollow capsules are inherently rigid and necessitated no further stabilization. By varying the sizes and shapes of the nanoparticles, we were able to tailor the pore diameters and pore size distributions on the surface of the capsules. Particles of high spherical uniformity with narrow size range generated colloidosomes with a mainly hexagonal close packed surface structure and narrow pore size, while particles of elliptical and uneven shape created colloidosomes with no surface order and an inconsistent structure. Synthesizing colloidosomes on the submicrometer scale and tailoring the pore shapes and diameters is a crucial step toward their application as a versatile encapsulation and release platform of active agents in the field of life sciences.

KEYWORDS: colloidosomes, microcapsules, metal oxide nanoparticles, thin films, lipids, drug delivery

Colloidosomes, hollow capsules formed via self-assembly of colloid particles on emulsion droplets, were first termed by Dinsmore et al.¹ and are based on a method originally pioneered by Velev et al.^{2–4} This type of semipermeable capsule possesses the potential to fabricate vesicles with tailored properties for the encapsulation and sustained release of active agents, such as drugs, flavors, or fragrances. Previous investigations have demonstrated colloidosome synthesis with various fine-tuned properties. These include increased mechanical stability,^{1,5–10} adjustable permeability,^{1,7,11–14} synthesis of pH^{7,11,15} and temperature¹⁶ responsive systems, and biocompatibility^{17–19} as well as the integration of materials with specific chemical and physical properties, including magnetic,^{19–21} catalytic,²² or semiconducting²³ characteristics. However, a major property that has not been reported to date is the assembly of colloidosomes with diameters below 1 μm . Due to altered resorption and membrane permeation mechanisms, synthesizing colloidosomes on the submicrometer

scale is a crucial step toward their application in life sciences, such as for the encapsulation of smaller biomolecules, targeted drug delivery,²⁴ or theranostic nanomedicine.^{25,26}

Control over capsule size, porosity, and mechanical stability are the key factors of colloidosome synthesis. Due to the interstitial spacing between the particles on the surface of the colloidosome, the permeability can be tailored by varying the size of the capsule-forming particles or by adjusting the shell thickness.²⁷ In addition, as is reported in literature, the porosity can be fine-tuned and the capsule's inherent rigidity can be enhanced by adding polymeric additives for a layer-by-layer assembly^{8,9,28} or to form a hydrogel core for a reinforcement of the capsules from within.^{29,30} The addition of polymers usually necessitates the use of potentially harmful ingredients though,

Received: May 17, 2013

Revised: July 29, 2013

limiting therefore their use specifically in the field of life sciences. The stability and porosity of colloidosomes can be further enhanced by merging the shell-forming particles by sintering.^{1,5,17,31} However, the utilization of sintering techniques to adjust the capsule's permeability and to increase the mechanical stability opposes various application limits for the encapsulation of active agents. Recently, Akartuna and co-workers³² introduced a general route for the assembly of inorganic capsules by using water-soluble surfactants that directly adsorbed to the colloidosome-forming nanoparticles. The capsules featured diameters in the range of several micrometers and exhibited an oil core, which is disadvantageous though for the encapsulation of most active agents that are only water-soluble.

Accordingly, demonstrated colloidosome sizes and the limitations created by previously described stabilization procedures highlight the need for a novel synthesis route to fabricate inherently rigid colloidosomes of small size with intrinsically developed nanopores. In this study, we present a straightforward synthesis route for the fabrication of colloidosomes at mild pH and ambient conditions with diameters below 1 μm , featuring tailorable nanometer-sized pores. Our preparation method is primarily inspired by the standard procedure given by Dinsmore et al.¹ and performed by adjusting the assembly route by Akartuna et al.³² Hereby, an emulsification step to prepare a water-in-oil emulsion is utilized to induce a self-assembly process of colloidosomes, which is subsequently followed by a centrifugation step to transfer the capsules from an organic into an aqueous phase.

Our hypothesized mechanical stabilization of the colloidosomes is based on our previous study,³³ where we demonstrated the growth of silica nanoparticle thin films at a planar water–oil (w-o) interface. The thin films were stabilized by adsorbing an oil-soluble surfactant (or lipid, e.g., stearic acid or stearyl amine) to the w-o interface, which carried an equal sign of charge as the colloid nanoparticles in aqueous media. We suggest that the lipid most likely acts as a local electrolyte at the w-o interface, thereby causing an attenuation of the electrostatic interactions between the charged nanoparticles, which in turn induced an agglomeration of the particles at the w-o interface. As a result, the nanoparticles and lipid formed a hybrid material thin film that consisted of only a few planar layers. Without the addition of lipids, the highly charged nanoparticles do not form thin films at the interface. Despite the marginal thickness, the thin film still exhibited an outstanding stability, which was evidenced by interfacial shear rheological measurements. On the basis of this finding, we transfer the method of a lipid-induced agglomeration of nanoparticles at a two-dimensional planar interface to a three-dimensional curved interface of water droplets, with the aim to obtain inherently rigid colloidosomes of submicrometer size. Submicrometer colloidosome synthesis is therefore realized by combination of lipids and nanoparticles at the w-o interface both carrying equal net charges. Thus, we use either negatively charged lipids with particles exhibiting a negative zeta-potential or positively charged lipids and nanoparticles featuring a positive zeta-potential.

A scheme of the submicrometer colloidosome synthesis route is illustrated in Figure 1. Prior to the colloidosome self-assembly, a water–oil based two-phase system is present (Figure 1A). We used different types of commercially available metal oxide nanoparticles in the aqueous phase, exhibiting either a positive or a negative surface charge at a pH between 4

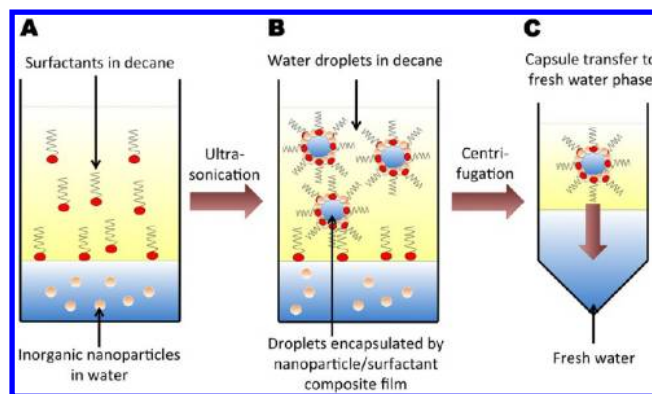


Figure 1. Submicrometer colloidosome preparation. (A) System before colloidosome generation consisting of a lipid oil solution (top) and an aqueous nanoparticle suspension (bottom). (B) Self-assembly of lipids and nanoparticles at the water–droplet oil interface after an ultrasound induced water-in-oil (w-o) emulsification. (C) Transfer of self-assembled colloidosomes to a fresh aqueous phase by centrifugation.

and 6. For colloidosome preparation, dispersions of 4 mL of 11.25 wt % SiO_2 (Ludox TMA), Al_2O_3 (Alu C), and Al_2O_3 coated SiO_2 (Ludox CL) colloids were prepared, as shown in Table 1. All experiments were conducted at pH values between 4 and 6 (see Table 1) and at ambient temperature.

Oil-soluble surfactants (Table 2) of intermediate length (2.4 nm) were used to tailor the physicochemical properties of the surface and to stabilize the nanoparticles that form the shell of the colloidosomes. Surfactants used included stearic acid, which possesses a carboxyl headgroup and carries a negative charge at the water–oil interface, as well as stearyl amine which features a primary amine headgroup, featuring a positive charge.

In our study, three colloid/lipid combinations of equally charged nanoparticles and lipids were employed to obtain submicrometer-sized colloidosomes. Ludox TMA, colloidal silica particles that exhibit a negative surface charge, were used with stearic acid, which induces a negative charge at the w-o interface at the pH of the nanoparticle dispersion. While Alu C as well as Ludox CL both feature a positive surface charge and were used with stearyl amine, that shows a positive charge at the w-o interface at the pH of the nanoparticle dispersion. Colloidosome formation proceeds through controlled agglomeration of the metal oxide particles at the droplet interfaces in the water-in-oil emulsion. When the metal oxide particles come into contact with the oil–water interface, which is populated by a Gibbs adsorption layer of lipid molecules with equal net charge, the surface charge interactions between the particles are blocked by the molecules and act as a local electrolyte. This leads to an agglomeration and a controlled self-assembly process of the metal oxide particles at the droplet interface. Using colloid/lipid combinations of opposite charges of the nanoparticles and lipids solely produces large agglomerates and is not applicable for colloidosome synthesis. The oil-soluble surfactants were diluted in 15 mL of decane with a molar concentration of 5 mM stearic acid and 4 mM stearyl amine, respectively. The decane phase was carefully layered on the aqueous colloidal dispersion, and the two-phase system was sonicated for 1 h in an ultrasound bath to generate homogeneous water-in-oil emulsions (Figure 1B).

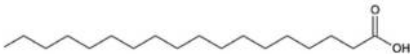

During the sonication procedure, the colloidosomes self-assemble in the decane phase. Here, the water droplets serve as templates for the shape and size of the colloidosomes. To

Table 1. Metal Oxide Nanoparticles and Corresponding Colloids Used for the Synthesis of Submicrometer Colloidosomes^a

metal oxide type	colloid name	average TEM diameter (nm)	pH of diluted colloid	surface charge at given pH	isoelectric point of metal oxide	nanoparticle shape
SiO ₂	Ludox TMA	25 ± 4	6	negative	~1	quasi spherical
Al ₂ O ₃	Alu C	12 ± 3	5	positive	~9	partially elliptical
Al ₂ O ₃ coated SiO ₂	Ludox CL	17 ± 3	4	positive	~9	quasi spherical

^aAnalyzing 100 randomly selected nanoparticles from TEM micrographs was the preferred method for the assessment of the nanoparticle diameters, since colloids showed a tendency for agglomeration in DLS measurement.

Table 2. Oil-Soluble Surfactants Used for the Interstitial Nanoparticle Stabilization during the Sub-Micrometer Colloidosome Synthesis

Surfactant	Chemical formula	Lewis formula	Molar mass (g/mol)	pK _a	Charge at w-o interface	Compatible colloid
Stearic acid	C ₁₈ H ₃₆ O ₂		284.48	4.9	negative	Ludox TMA
Stearyl amine	C ₁₈ H ₃₉ N		269.51	10.6	positive	Alu C, Ludox CL

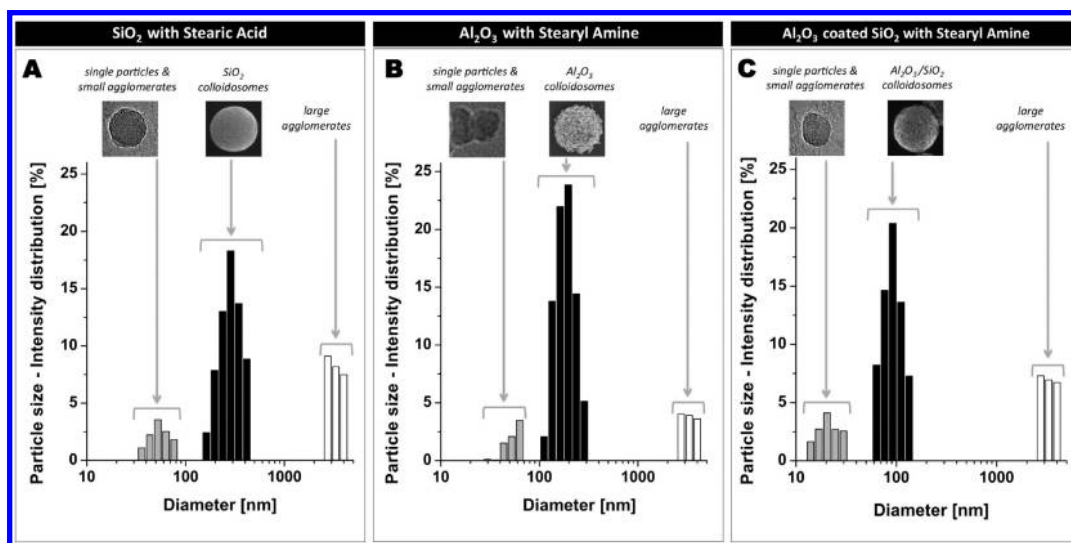


Figure 2. DLS intensity distribution results for (A) SiO₂ (LudoxTMA), (B) Al₂O₃ (AluC), and (C) Al₂O₃ coated SiO₂ (LudoxCL) colloidosomes after centrifugation to a fresh aqueous phase, all showing a trimodal particle distribution.

regain clear phase boundaries between aqueous as well as organic phases and to separate larger colloidosomes and aggregates from submicrometer colloidosomes by sedimentation, the mixtures were left unperturbed for 1 h after sonication. Afterward, 10 mL of the organic phase containing the submicrometer colloidosomes were carefully poured onto 10 mL of fresh Millipore water in 50 mL of centrifugation tubes. In order to transfer the colloidosomes from the organic to the aqueous phase, the system was centrifuged for 30 min at 5000 rpm (Figure 1C). The centrifugation of colloidosomes to a fresh aqueous phase also serves as a washing step, causing colloidosomes and excess lipid molecules from the organic phase to be separated. After centrifugation, the decane phase was carefully removed from the centrifugation tubes, and the aqueous phase containing the colloidosomes was collected. To study the colloidosomes via transmission electron microscopy to analyze their interior build up, small portions were freeze-dried for five days at -35 °C.

Colloidosomes were characterized via dynamic light scattering (DLS), zeta-potential measurements, scanning electron microscopy (SEM), and conventional (CTEM) as well as scanning transmission electron microscopy (STEM). The hydrodynamic size distributions of the varying colloidosome types were assessed via the analysis of DLS intensity distribution results (Figure 2). All three specimen show a trimodal particle distribution, indicating a coexistence of colloidosomes, single particles, small agglomerates and few larger aggregates. The main peak of all three samples originates from colloidosomes featuring diameters in the range of about 100 nm up to a few hundred nanometers, confirming the submicrometer size of all three colloidosome types. The size distributions of all three colloidosome types correspond to a nonmonomodal Gaussian distribution. In addition, we used the cumulant method to analyze the DLS data, finding diameters of (420 ± 160) nm for the SiO₂, (230 ± 60) nm for the Al₂O₃, and (200 ± 140) nm for the Al₂O₃ coated SiO₂ colloidosomes. The polydispersity index for all measurements was below 0.25.

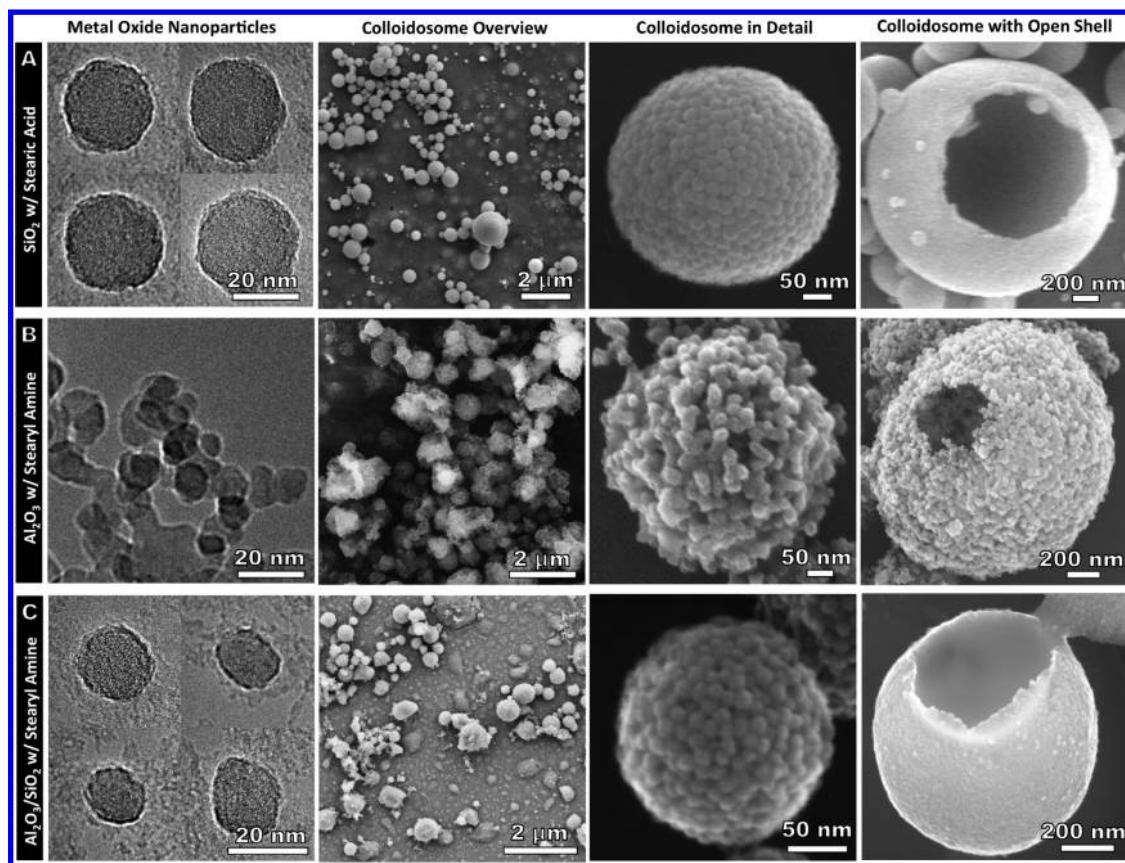


Figure 3. TEM micrographs of metal oxide nanoparticles (first column), SEM overview images of synthesized colloidosomes (second column), and detailed illustrations of representative intact submicrometer colloidosomes (third column) as well as colloidosomes with a partially open shell showcasing a hollow interior (fourth column). (A) SiO_2 with stearic acid based colloidosomes, which show a highly spherical shape in analogy to their building block nanoparticles. (B) Al_2O_3 colloidosomes prepared with stearyl amine which exhibit a less ideally spherical structure in correlation to the partially elliptical shaped Al_2O_3 nanoparticles. (C) Colloidosomes synthesized from Al_2O_3 coated SiO_2 nanoparticles and stearyl amine which, similar to the SiO_2 with stearic acid based colloidosomes, comprise a mainly spherical shape.

The fact that the colloidosomes maintain their submicrometer size after centrifugation emphasizes the high stability of the capsules. The preparation of colloidosomes using the method described above is therefore highly reproducible and yields inherently rigid colloidosomes for all three colloid types with diameters below $1\ \mu\text{m}$. Zeta-potential measurements indicated a high electrostatic stability of the colloidosomes in the aqueous solution after centrifugation. As expected, we found zeta-potential values that correspond to the metal oxide nanoparticles with $-40\ \text{mV}$ for the SiO_2 , $+43\ \text{mV}$ for the Al_2O_3 , and $+75\ \text{mV}$ for the Al_2O_3 coated SiO_2 colloidosomes. The strength of the zeta-potential is high enough to prevent the colloidosomes from agglomeration.

Similar to the DLS studies, we found colloidosomes that featured diameters below $1\ \mu\text{m}$ by using SEM and TEM. Figure 3 shows TEM micrographs of the colloidosome-forming nanoparticles and SEM images of their corresponding colloidosomes. The first column in Figure 3 illustrates the metal oxide particles, which were drop-casted onto TEM graphene grids, after diluting the colloids from 11.25 wt % to 0.005 wt % and desagglomerating the suspension via ultrasonication for 1 h. The Ludox TMA (SiO_2) and Ludox CL (Al_2O_3 coated SiO_2) colloids feature particles of a mainly spherical shape with average diameters of 25 and 17 nm, respectively. In contrast, the Alu C colloid (Al_2O_3) could not be desagglomerated. Accordingly, no individual particles were found on the graphene grid. The Alu C colloid particles are of

partially elliptical shape and feature a mean diameter of 12 nm. In addition to using TEM micrographs to measure the diameters of single particles we also performed DLS measurements for all three colloid types. While Ludox TMA showed a monomodal DLS intensity result corresponding closely to the measured diameters from TEM pictures, Ludox CL showed some aggregates and Alu C indicated a strong tendency for agglomeration. Apparently, mainly individual and nonagglomerated colloidal particles formed colloidosomes.

The metal oxide particles form a large number of colloidosomes, as shown in the low resolution overview images in the second column of Figure 3. For SEM morphology studies and to control the specimen structures prior to the freeze-drying process, the colloidosomes were drop-casted onto silicon wafers directly from the decane phase. Representative capsules are depicted in the third column. The colloidosomes based on SiO_2 with stearic acid (Figure 3A) show highly spherical shapes in analogy to their building block nanoparticles. Al_2O_3 colloidosomes prepared with stearyl amine (Figure 3B) exhibit a less ideal spherical structure. Colloidosomes synthesized from Al_2O_3 coated SiO_2 (Figure 3C) nanoparticles and stearyl amine, similar to colloidosomes based on SiO_2 with stearic acid, feature a mainly spherical shape. During the drying process, the shell of some of the capsules lost their structural integrity evidencing the interior build up of these colloidosomes to be primarily hollow. Hollow colloidosomes were most easily observed with larger than

average microcapsules in the SEM studies (Figure 3—fourth column), while we found smaller hollow capsules using STEM images (see below).

The colloidosomes' shell and its pores potentially impact the diffusion path of an active agent and therefore the release from the capsules' cores. Hexagonal closed packing (hcp) provides the smallest possible pore size in colloidosomes and can be ideally realized via the self-assembly of spherical nanoparticles of narrow size distribution. Figure 4A illustrates a SiO₂ colloidosome featuring a closed packed surface structure in more detail. Magnification (Figure 4-A.1) of the surface shows a spot with hcp, emphasizing the high order of the building-

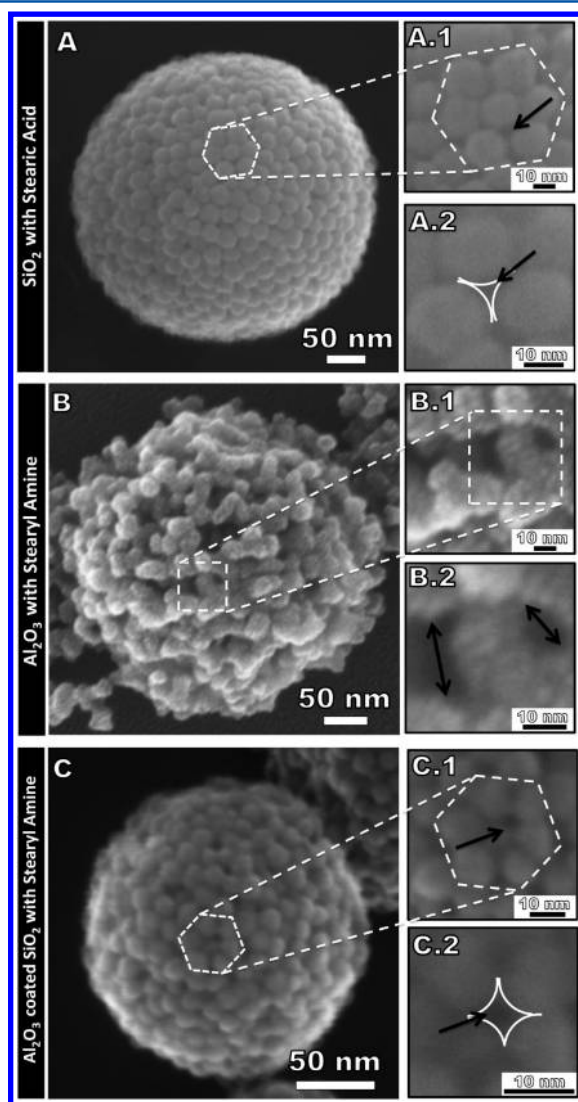


Figure 4. SEM micrographs illustrating the topological properties of the varying colloidosome types, including a detailed view of several nanopores. (A) SiO₂ colloidosome, exhibiting a highly ordered packing of the single nanoparticles. The two-dimensional surface packing is primarily hexagonally closed packed (hcp), depicted more closely in the magnification (A.1), leading to small pore sizes (A.2) with a narrow size distribution. (B) Al₂O₃ colloidosome shows no order in the individual nanoparticle packing (B.1), featuring tight as well as wide pores (B.2) on the surface of the colloidosome. (C) Al₂O₃ coated SiO₂ colloidosome displaying a mostly dense packed surface structure with areas featuring hcp (C.1), leading to small pore sizes (C.2).

block particles of this colloidosome type, which results in small pore sizes (Figure 4-A.2).

By image analysis and measurement of 100 randomly selected pores on the surface, the average pore size of the SiO₂ colloidosomes was assessed to be 7.9 nm, with a standard deviation of 2 nm. This measured average diameter correlates well to a calculated pore size of 5.2 nm, for a hcp colloidosome with the assumption of individual particles to be spherically shaped and of the same size (we used average TEM particle diameters from Table 1 for calculations). The variance between the measured and calculated results is most likely due to marginal imperfections in the arrangement of the nanoparticles, causing some inhomogeneity in the particle packing and a nonmonomodal pore size distribution. In contrast, the Al₂O₃ colloidosomes show a significantly inferior surface packing of the particles (Figure 4B). Magnifying the surface (Figure 4-B.1) reveals a substantially unordered packing, which explains the larger measured pore sizes and a broader pore size distribution (Figure 4-B.2) on the order of 13.7 ± 9 nm. This observation might be correlated to the nonspherical shapes of the Al₂O₃ particles (see Figure 3B) and their highly inhomogeneous packing on the surface. A calculation with spherical particles yielded a smallest theoretical pore size of 2.5 nm for this colloidosome type. Similar to the capsules derived from SiO₂ particles, the Al₂O₃ coated SiO₂ colloidosomes (Figure 4C) display a likewise hcp surface structure (Figure 4-C.1) with mostly small pores (Figure 4-C.2). The average measured pore size of 4.2 ± 1 nm correlates very well to the calculated result of 3.5 nm. Potentially all three colloidosome types exhibit pore sizes in the dimension of small biomolecules, wherefore these microcapsules should possess the ability for the storage and sustained release of various molecular species. Table 3 summarizes the structural properties of the different colloidosome types.

As mentioned above, a small portion of the colloidosomes was freeze-dried and prepared on TEM graphene grids. For an additional characterization of the inner capsule structure, we used CTEM and STEM micrographs (Figure 5—first and second column) and analyzed their HAADF (high angle annular dark field) intensity distribution (Figure 5—third column). For the present colloidosomes the HAADF intensity in STEM can be expected to increase monotonically with specimen thickness. Therefore, hollow colloidosomes and solid capsules can be easily differentiated by comparing line scans taken from their equators.

The HAADF profile in Figure 5-A.1 shows a continuous intensity gain toward the center of the SiO₂ colloidosome, which points to the presence of a solid capsule. In contrast, the HAADF intensity in Figure 5-A.2 declines towards the center after reaching a peak on the outer edge of the colloidosomes, which clearly indicates a hollow capsule. We were able to find various solid as well as hollow Ludox TMA colloidosomes that are inherently rigid and maintained their spherical structure after the freeze-drying process. Like hollow colloidosomes, solid capsules eventually also possess the ability to store active agents. Since active agents are stored in the aqueous core or in the interstitial spaces between nanoparticles, solid capsules and hollow colloidosomes will most likely show a substantially different release kinetic behavior. Through a potential control of the ratio of solid capsules and hollow colloidosomes in a specimen, the release of kinetic behavior may potentially be tailored for specific applications. Al₂O₃ colloidosomes exhibited an inconsistent HAADF profile (Figure 5B) while the line scan

Table 3. Structural Properties of Submicrometer Colloidosomes^a

colloidosome type	cumulant size distribution (nm)	zeta potential (mv)	determined average pore size (nm)	calculated smallest pore size for hcp (nm)	surface structure
SiO ₂	420 ± 160	−40 ± 2	7.9 ± 2	5.1	mainly hcp
Al ₂ O ₃	230 ± 60	+43 ± 11	13.7 ± 9	2.5	unordered
Al ₂ O ₃ coated SiO ₂	200 ± 140	+75 ± 6	4.2 ± 1	3.5	partially hcp

^aThe colloidosome size distributions were gained via DLS measurements and calculated with the cumulative method. The zeta potential was measured via electrophoretic light scattering. Surface pore sizes of the colloidosomes were assessed by measuring 100 pores on the surface of the colloidosomes from SEM images and by a calculation for spherical particles on a hcp surface.

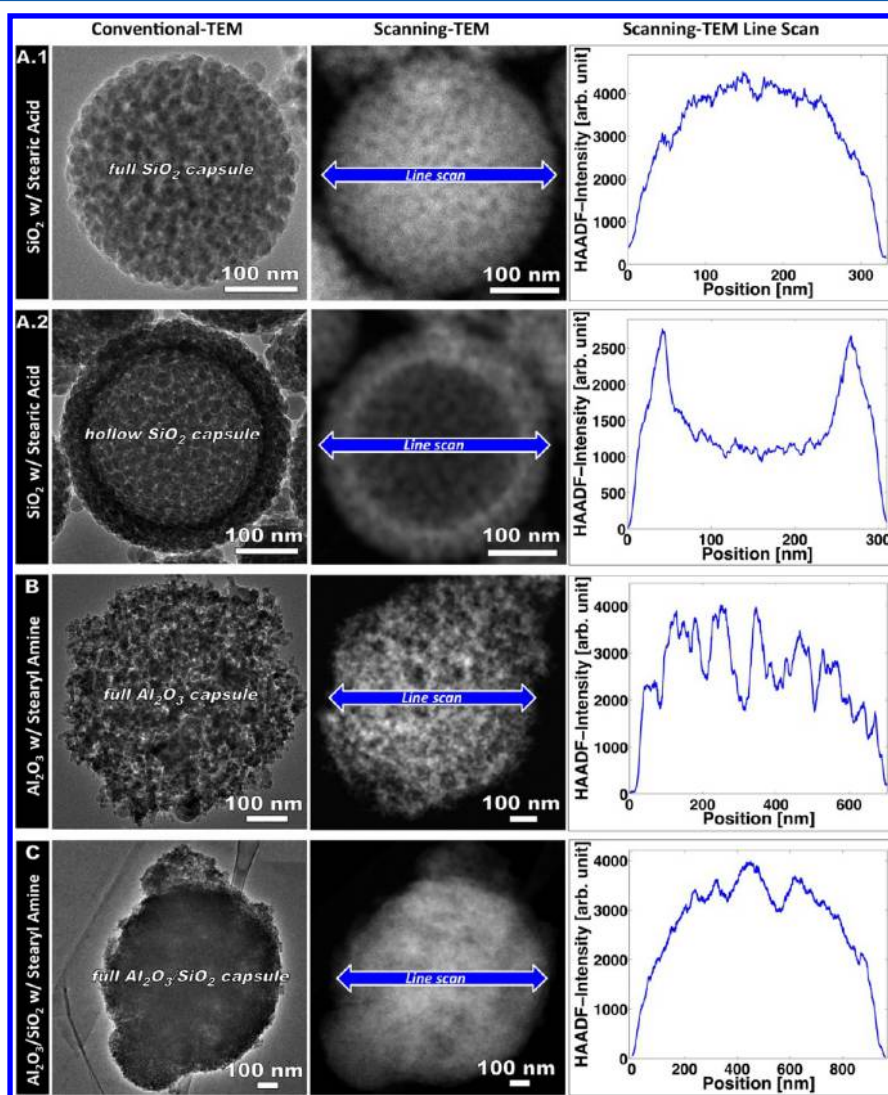


Figure 5. TEM characterization of freeze-dried colloidosomes. Left column: Representative conventional-TEM micrographs of varying colloidosome types. Middle column: STEM micrographs with an indicated line-scan for the characterization of the interior colloidosome structure. Right column: STEM line-scan graphs, quantitatively describing the interior colloidosome structure. (A) Image shows a SiO₂ colloidosome filled with particles (A.1) in comparison with a hollow SiO₂ colloidosome (A.2). (B) Al₂O₃ colloidosome that partially lost its spherical shape during the freeze-drying process, showing a partially ragged structure in the STEM line scan graph. (C) Al₂O₃ coated SiO₂ colloidosome filled with particles.

points to a highly ragged structure of the capsules. Also, while silica nanoparticles have been proven to be nontoxic in most cases³⁴ and are extensively studied as drug-delivery vesicles,³⁵ the toxicological effects of nanoparticles featuring an alumina surface layer are still being investigated.³⁶

The loss of the structural integrity of these colloidosomes is assumed to be due to the freeze-drying process, causing fracture of those colloidosomes that are structurally weakened due to their irregularity. Most Al₂O₃ coated SiO₂ colloidosomes

(Figure 5C) comprise a HAADF profile similar to the solid SiO₂ colloidosomes. In comparison to the SEM studies, where we found a high number of hollow colloidosomes, the STEM micrographs and line-scans only revealed a marginal amount of hollow capsules. The low number of hollow capsules is most likely caused by the freeze-drying process, where a high Laplace pressure may rupture the hollow colloidosomes from inside, leaving mainly capsules filled with particles.

In summary, we present a straightforward method for the preparation of submicrometer-sized colloidosomes with tailorable nanopores. Capsule formation was carried out at mild pH, ambient temperature, and without the use of hazardous chemicals. In combination with a lipid that carries the same net charge at an oil–water interface as the colloidosome-forming particles in aqueous media, we were able to synthesize colloidosomes with positive and negative zeta potentials. The capsules are stable both in organic as well as in aqueous environments. The different colloidosome types are therefore potentially suitable for the encapsulation of positively or negatively charged biomolecules. By varying the sizes and shapes of the nanoparticles, we were able to tailor the pore diameters and pore size distributions on the surface of the capsules. It was observed that particles of high spherical uniformity with a narrow size range generate colloidosomes with a regular surface structure and narrow pore sizes. In contrast, particles of elliptical and uneven shape created colloidosomes with no surface order and an inconsistent structure. Tailoring the size of the colloidosome nanopores potentially allows the controlled release of encapsulated active agents of different size, such as proteins, antibiotics, or chemotherapeutics.

EXPERIMENTAL SECTION

Chemicals. Silicon dioxide colloid (Ludox TMA), aluminum oxide coated silicon dioxide colloid (Ludox CL), stearic acid, stearyl amine (all Sigma Aldrich, Munich, Germany), and aluminum oxide powder (Alu C, Evonik, Frankfurt, Germany) were purchased at analytical grade purity and used without any further purification.

Dynamic Light Scattering. Dynamic light scattering (DLS) was measured using a Beckman-Coulter DelsaNanoC. A sample volume of 1.4 mL was filled in Sarstedt fluorescence cuvettes (polystyrene, $d = 1$ cm, Sarstedt, Nümbrecht, Germany). The experiments were carried out at the backscattering angle of 165° . The data was evaluated via intensity distribution as well as the cumulant method. The software of the DLS device does not include the option to enter a refractive index for solid materials to calculate the number and volume distribution, as why we used the intensity distribution and cumulant intensity results to assess the colloidosome sizes.

Zetapotential Measurements. Zetapotential measurements were also done using the Beckman Coulter DelsaNanoC. A sample volume of 5 mL was filled in a Flow Cell and equilibrated with the same conditions mentioned in the Dynamic Light Scattering section. Here the measurements were done at the scattering angle of 15° . The measurement time was 130 s per repetition.

Scanning Electron Microscopy. Scanning electron microscopy (SEM) images were acquired using a Zeiss Auriga40 and a Zeiss Supra40. Samples were either deposited directly from the organic phase or prepared from colloidosomes from the aqueous phase, which underwent freeze-drying. Colloidosomes from the organic phase were prepared on silicon substrates and freeze-dried colloidosomes on carbon sticky tape. The samples did not require a sputter coating.

Transmission Electron Microscopy. Transmission electron microscopy (TEM) was carried out using an FEI Titan 80/300 kV equipped with a cs-corrector for spherical aberration of the objective lens at 300 kV. Samples of freeze-dried colloidosomes were deposited on CVD graphene film coated copper grids from Graphene Supermarket (New York, USA).

Image Analysis. The software tool ImageJ was used to determine the average diameters of the metal oxide nanoparticles, where 100 individual particles were measured for each colloid type. Furthermore, the pore size range of the colloidosomes was assessed by measuring 100 pores for each colloidosome type.

AUTHOR INFORMATION

Corresponding Author

*Fax: +49 421 218 64932. E-mail: michael.maas@uni-bremen.de.

Notes

The authors declare no competing financial interest.

ACKNOWLEDGMENTS

We thank Marco Schowalter, Knut Müller, and Jan Köser for their assistance in the experimental work. We are grateful for the support of the German Research Foundation (DFG MA4795/5-1).

REFERENCES

- (1) Dinsmore, A. D.; Hsu, M. F.; Nikolaidis, M. G.; Marquez, M.; Bausch, A. R.; Weitz, D. A. *Science* **2002**, 298, 1006–1009.
- (2) Velev, O. D.; Furusawa, K.; Nagayama, K. *Langmuir* **1996**, 12, 2374–2384.
- (3) Velev, O. D.; Furusawa, K.; Nagayama, K. *Langmuir* **1996**, 12, 2385–2391.
- (4) Velev, O. D.; Nagayama, K. *Langmuir* **1997**, 13, 1856–1859.
- (5) Hsu, M. F.; Nikolaidis, M. G.; Dinsmore, A. D.; Bausch, A. R.; Gordon, V. D.; Chen, X.; Hutchinson, J. W.; Weitz, D. A.; Marquez, M. *Langmuir* **2005**, 21, 2963–2970.
- (6) Ao, Z.; Li, Z.; Zhang, G.; Ngai, T. *Colloids Surf., A* **2011**, 384, 592–596.
- (7) Cayre, O. J.; Hitchcock, J.; Manga, M. S.; Fincham, S.; Simoes, A.; Williams, R. A.; Biggs, S. *Soft Matter* **2012**, 8, 4717–4724.
- (8) Rossier-Miranda, F. J.; Schroën, K.; Boom, R. *Food Hydrocolloids* **2012**, 27, 119–125.
- (9) Mak, W. C.; Bai, J.; Chang, X. Y.; Trau, D. *Langmuir* **2009**, 25, 769–775.
- (10) Thompson, K. L.; Armes, S. P. *Chem. Commun.* **2010**, 46, 5274–5276.
- (11) Miguel, A. S.; Behrens, S. H. *Soft Matter* **2011**, 7, 1948–1956.
- (12) Kim, J.-W.; Fernández-Nieves, A.; Dan, N.; Utada, A. S.; Marquez, M.; Weitz, D. A. *Nano Lett.* **2007**, 7, 2876–2880.
- (13) Lee, D.; Weitz, D. A. *Adv. Mater.* **2008**, 20, 3498–3503.
- (14) Fielding, L. A.; Armes, S. P. *J. Mater. Chem.* **2012**, 22, 11235–11244.
- (15) Shah, R. K.; Kim, J.-W.; Weitz, D. A. *Langmuir* **2010**, 26, 1561–1565.
- (16) Lawrence, D. B.; Cai, T.; Hu, Z.; Marquez, M.; Dinsmore, A. D. *Langmuir* **2007**, 23, 395–398.
- (17) Laib, S.; Routh, A. F. *J. Colloid Interface Sci.* **2008**, 317, 121–129.
- (18) Keen, P. H. R.; Slater, N. K. H.; Routh, A. F. *Langmuir* **2012**, 28, 16007–16014.
- (19) Sander, J. S.; Studart, A. R. *Langmuir* **2011**, 27, 3301–3307.
- (20) Duan, H.; Wang, D.; Sobal, N. S.; Giersig, M.; Kurth, D. G.; Möhwald, H. *Nano Lett.* **2005**, 5, 949–952.
- (21) Samanta, B.; Patra, D.; Subramani, C.; Ofir, Y.; Yesilbag, G.; Sanyal, A.; Rotello, V. M. *Small* **2009**, 5, 685–688.
- (22) Wu, C.; Bai, S.; Ansoorge-Schumacher, M. B.; Wang, D. *Adv. Mater.* **2011**, 23, 5694–5699.
- (23) Lin, Y.; Skaff, H.; Emrick, T.; Dinsmore, A. D.; Russell, T. P. *Science* **2003**, 299, 226–229.
- (24) Haglund, E.; Seale-Goldsmith, M.-M.; Leary, J. F. *Ann. Biomed. Eng.* **2009**, 37, 2048–2063.
- (25) Janib, S. M.; Moses, A. S.; MacKay, J. A. *Adv. Drug Delivery Rev.* **2010**, 62, 1052–1063.
- (26) Ambrogio, M. W.; Thomas, C. R.; Zhao, Y.-L.; Zink, J. I.; Stoddart, J. F. *Acc. Chem. Res.* **2011**, 44, 903–913.
- (27) Rosenberg, R. T.; Dan, N. R. *J. Colloid Interface Sci.* **2011**, 354, 478–482.
- (28) Li, J.; Stöver, H. D. H. *Langmuir* **2010**, 26, 15554–15560.
- (29) Cayre, O. J.; Noble, P. F.; Paunov, V. N. *J. Mater. Chem.* **2004**, 14, 3351–3355.

- (30) Wang, C.; Liu, H.; Gao, Q.; Liu, X.; Tong, Z. *ChemPhysChem* **2007**, *8*, 1157–1160.
- (31) Yow, H. N.; Routh, A. F. *Langmuir* **2009**, *25*, 159–166.
- (32) Akartuna, I.; Tervoort, E.; Studart, A. R.; Gauckler, L. J. *Langmuir* **2009**, *25*, 12419–12424.
- (33) Maas, M.; Ooi, C. C.; Fuller, G. G. *Langmuir* **2010**, *26*, 17867–17873.
- (34) Fruijtier-Pöloth, C. *Toxicology* **2012**, *294*, 61–79.
- (35) Yang, P.; Gai, S.; Lin, J. *Chem. Soc. Rev.* **2012**, *41*, 3679–3698.
- (36) Wehling, J.; Volkmann, E.; Grieb, T.; Rosenauer, A.; Maas, M.; Treccani, L.; Rezwan, K. *Environ. Pollut.* **2013**, *176*, 292–299.